MULTI-FIELD STABILIZED FINITE ELEMENT APPROXIMATIONS FOR QUASI-NEWTONIAN FLUID FLOWS

Flávia Zinani[1], fzinani@unisinos.br
Mechanical Engineering Department
UNISINOS – Universidade do Vale do Rio dos Sinos
Av. Unisinos, 950 – 93.022-000 – São Leopoldo, RS, Brazil.
UCS – Universidade de Caxias do Sul
R. Francisco Getúlio Vargas, 1130 – 95.070-560 – Caxias do Sul, RS, Brazil.

Sérgio Frey, frey@mecanica.ufrgs.br
Laboratory of Computational and Applied Fluid Mechanics (LAMAC), Mechanical Engineering Department
UFRGS – Federal University of Rio Grande do Sul
R. Sarmento Leite, 425 – 90050-170 – Porto Alegre, RS, Brazil.

Abstract. *This work aims the study of inelastic non-Newtonian flows employing quasi-Newtonian fluid models sensitive to the flow type. These models use a kinematic parameter of flow classification and the flow curves in viscometric and extensional regimes to represent the fluid behavior from pure shear to pure extensional flow regions in a weighted manner. Multi-field formulations with strain rate, pressure and velocity as primal variables (**D**-p-**u**), are a quite attractive alternative to numerical approximations for quasi-Newtonian fluid flows, because they allow the use of low-order elements with a still good precision in the determination of the flow classification parameter. In the numerical approximations undertaken in this article, a Galerkin-least-squares-like stabilized method has been used in order to circumvent the compatibility conditions involving the finite element sub-spaces for the primal variables. Besides, the GLS-like strategy was able to stabilize the intrinsic numerical oscillations due the asymmetric features of advective operators in the motion equation. Some two-dimensional numerical simulations were shown to validate the computational implementation of the introduced multi-field stabilized formulation. Numerical investigations of quasi-Newtonian fluids through a plane contraction have been carried out. The Carreau equation was employed to model both pure viscometric and extensional behaviors, and the values of the power-law parameter were varied from 0.2 up to 2.5 in pure extension, in many combinations. The high viscosity zones near the contraction and the normal stresses and velocity profiles were discussed, showing the physical meaning of flow-type sensitive models. The stabilized method have proven to be stable and able to generate comprehensive approximations for all simulated problems.*

Keywords: Flow classification, Flow-type sensitive fluids, Quasi-Newtonian fluids, Multi-field formulations, Galerkin least-squares.

1. INTRODUCTION

Non-Newtonian materials are present in a broad class of fluid applications in different engineering fields, such as emulsions, polymer melts and solutions, food products, biological fluids, drilling muds and heavy oil from the petroleum industry, asphalts and so many others.

The limited performance of some classical differential viscoelastic fluid models, which may failure either in generality or in the quantitative representation of rheological experimental data, added to the difficulty in the implementation of such models with usual numerical methods, has encouraged non-Newtonian fluid researchers to look for simpler constitutive models still capable to characterize fluid behavior in relevant engineering applications. The experimental verification of the distinct behavior of non-Newtonian fluids in pure shear and extensional flows – namely shear-thinning and extensional thickening – along with the prediction of fluid behavior in mixed-type flows has been some of the first questions to be thought of. Flow classification criteria, since the pioneer work of Astarita (1979), have introduced a theoretical starting point for the identification of such an application. Later, the works of Schunk and Scriven (1990), Thompson and Souza Mendes (2005) and references therein, have discussed some of the major quests related to flow-classification, and formed the basis for the proposition of flow-type sensitive flow models, which have become an interesting alternative for industrial non-Newtonian applications (see Thompson *et al.*, 1999; Ryssel and Brunn, 1999). Most of the flow-type sensitive models have the features of predicting complex fluid behavior and being made of simple mathematical equations, hence they are called quasi-Newtonian.

The quasi-Newtonian equations have the advantage to allow simultaneously both shear-thinning behavior in pure shear flows and extensional-thickening in pure extensional flows and also to weight between these two behaviors in mixed flows. In the quasi-Newtonian model addressed in this work, the viscosity function depends on kinematic parameters related to the flow type.

---

[1] Corresponding author.

The quasi-Newtonian fluid flows considered in this article have been approximated via a multi-field stabilized method based on the Galerkin least-squares (GLS) strategy. This method was employed to avoid undesirable numerical pathologies – such as spurious oscillations and locking – to which the classical Galerkin formulation would be susceptible. Hence, the stabilized method employed herein has the ability to circumvent the *inf-sup* compatibility conditions involving the finite element sub-spaces for velocity-pressure – the so-called Babuška-Brezzi condition – and for stress-velocity fields. In addition, the method is still able to generate stable approximations for flows subjected to high geometrical and material non-linearities, preserving good accuracy properties (Franca and Frey, 1992). This is achieved by adding residual-based terms to the classic Galerkin formulation, retaining its weighted residual structure and not damaging its consistency.

In this article, quasi-Newtonian fluid flows through a four-to-one sudden contraction with a rounded corner have been simulated. The numerical simulations have been performed by a multi-field stabilized method with strain rate, velocity and pressure (**D**-p-**u**) as primal variables. For low Deborah flows, four different flow-type sensitive fluids have been considered: a Newtonian fluid, a shear-thinning fluid only in pure shear flows, an extensional-thickening fluid only in extensional flows and a shear-thinning and extensional-thickening fluid. For all flows, the distribution of the flow classifier has been evaluated, all of them showing extensional region near the contraction plane and pure shear flows far away the contraction. The velocity, pressure, stress and viscosity fields have also been studied. The normal stress growth in the contraction zone could be detected, and the velocity profiles in these zones have been studied. All results showed good agreement with the literature and were found physically comprehensive, indicating that both the numerical method and the constitutive model could be of great use.

2. THE MECHANICAL MODEL

Although Cauchy theorem describes the form of contact forces for any continuous mechanical body, the way in which materials deform under arbitrary dynamic conditions is not stated by this theorem. In addition, the behavior of continuous bodies drastically differs with respect to the relation between internal contact forces (accounted by the stress tensor, $\mathbf{T} = \boldsymbol{\tau} + p\mathbf{1}$) and their motion and deformation. This relation is described by the material constitutive equations.

The constitutive equation for the extra-stress tensor, $\boldsymbol{\tau}$, used in this work, is of a purely viscous fluid, so the model may be considered one of a *quasi-Newtonian fluid*. This model is given by

$$\boldsymbol{\tau} = 2\,\eta\,(R_r\,,\,II_{\mathbf{D}})\,\mathbf{D} \tag{1}$$

where the viscosity, η, is a function of the flow classifier, R_r, and of the second invariant of strain rate tensor $\mathbf{D}$, $II_{\mathbf{D}}$.

The flow classification function proposed by Thompson and Souza Mendes (2005) has been adopted with some light modifications. The original kinematic flow classifier R_R assumes the value of 0 for pure extensional flows, 1 for pure shear flows and tends to infinitive for rigid body motion. Following the idea of Ryssel and Brunn (1999), one may build a bounded flow classifier, R_r, that has the maximum value of 2 when the kinematics is the one of rigid body motion, keeping the same values for pure shear and extension:

$$R_r = \frac{2\,R_R}{1 + R_R} \tag{2}$$

The viscosity function considered herein has been given by a weighted mean between the shear viscosity, η_s, and the extensional viscosity, η_{ex}, both of them independently constructed according the Carreau equation,

$$\begin{aligned}
\eta &= \eta_s^{f(R_r)}\,\eta_{ex}^{(1-f(R_r))} \\
\eta_s &= \eta_0\,(1 + (\lambda_s\,\dot{\gamma})^2)^{(n_s-1)/2} \\
\eta_{ex} &= \eta_0\,(1 + (\lambda_{ex}\,\dot{\gamma})^2)^{(n_{ex}-1)/2}
\end{aligned} \tag{3}$$

in which η_0 is the zero-shear-rate viscosity, $\dot{\gamma}$ the magnitude of tensor $\mathbf{D}$, $\dot{\gamma} = (2\,\mathrm{tr}\mathbf{D}^2)^{1/2}$. The shear-thinning or extensional-thickening effects were controlled by the shearing power-law index, n_s, <1, and the extensional one, $n_{ex} > 1$, and the parameter λ_s and λ_{ex} were, respectively, time constants equal to the reciprocals of shear and extensional rate values, for which the power-law regions of Eq. (3) begin. When the flow classifier is greater than one, $R_R > 1$, *i. e.*, the flow tends to become a rigid body motion, the viscosity function defined by Eq. (3) goes to zero, as required by this kind of motion (Souza Mendes et al., 1995).

For the function $f(R_r)$ employed in Eq. (3), the function proposed by Ryssel and Brunn (1999) has been employed,

$$f(R_r) = \frac{3\sin^4(R_r\pi/2)}{1+2\sin^4(R_r\pi/2)} \tag{4}$$

The definition for the function $f(R_r)$ given by Eq. (4) aims to smooth the flow classifier distribution, weighting the geometric mean of shear and extensional viscosity functions defined by Eq. (3) – see Fig. 1, for the function $f(R_r)$ behavior in the interval $0 \le R_r \le 2$.
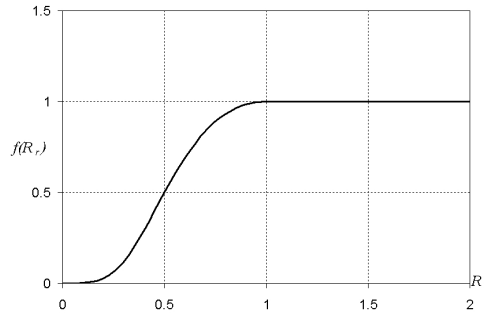
Figure 1. Function $f(R_r)$ versus R_r.

Hence, the viscosity function for the flow-type sensitive fluids considered herein may be presented as an elevation plot on a plane spanned by the flow classifier, R_r, and the magnitude of the shear rate tensor, $\dot\gamma$ – as it illustrated in Fig. 2. This figure mainly illustrates the influence the flow classifier R_r on the viscosity behavior. First, for extension-dominated flows, Eq. (3) prescribes viscosity increasing with the increase of strain rate. Second, for values of R_r very closed to pure shear flows, a viscosity decay may be observed. At last, for values comprised between $1 < R_r < 2$, the more R_r increases, the more Eq. (3) prescribes a viscosity decay, as suggested by Astarita (1991).
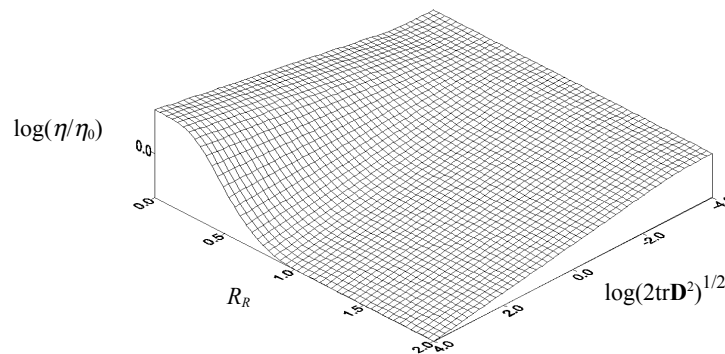
Figure 2. Viscosity elevation plot on the R_R x $\dot\gamma$ plane.

3. FINITE ELEMENT MODELING

The fluid flows studied in this article have been defined in an open bounded domain $\Omega \subset \mathfrak{R}^{N=2,3}$ with polygonal boundary Γ such that,

$$\begin{aligned} \Gamma &= \overline{\Gamma}_h \cup \overline{\Gamma}_h \\ \Gamma_g \cap \Gamma_h &= \emptyset \quad, \Gamma_g \ne \emptyset \end{aligned} \tag{5}$$

where Γ_g is the portion of Γ on which the Dirichlet boundary conditions were imposed and Γ_h the portion of Γ where the Neumann boundary conditions were prescribed.

3.1 The (d-*p*-u) multi-field formulation

From the momentum and mass balance equations for a continuous body (Gurtin, 1981) coupled with the constitutive equation for the extra stress tensor defined by Eq. (1), a multi-field boundary value problem, for steady-state flows of purely viscous fluids, may be stated as: *given the body force* $\mathbf{b}:\overline{\Omega}\subset R^N\to R^N$, *boundary conditions* $\mathbf{u}_g:\Gamma_g\subset R^{N-1}\to R^N$ *and* $\mathbf{t}_h:\Gamma_h\subset R^{N-1}\to R^N$ *find the triple* (**d**-*p*-**u**) *such that*

$$\rho[\nabla\mathbf{u}]\mathbf{u}-2\eta(R_r,II_{\mathbf{D}})\,\text{div}\,\mathbf{d}-2[\mathbf{d}]\nabla(\eta(R_r,II_{\mathbf{D}}))+\nabla p=\rho\mathbf{b} \qquad \text{in } \Omega$$
$$\mathbf{d}-\mathbf{D}(\mathbf{u})=0 \qquad \text{in } \Omega$$
$$\text{div}\,\mathbf{u}=0 \qquad \text{in } \Omega \qquad (6)$$
$$\mathbf{u}=\mathbf{u}_g \qquad \text{on } \Gamma_g$$
$$[-p\mathbf{1}+2\eta(R_r,II_{\mathbf{D}})\mathbf{D}(\mathbf{u})]\mathbf{n}=\mathbf{t}_h \qquad \text{on } \Gamma_h$$

where **u** is the fluid velocity, *p* the pressure, ρ the mass density, **d** and **D(u)** are alternative notations for the strain-rate tensor – **d** is the variable srain-rate and **D(u)** is the function of the velocity **u** – **1** the unity tensor, **n** the outward unity vector, $\mathbf{t}_h$ the stress vector given by the decomposition of the stress tensor **T** in spheric and deviatoric portions, **T**=τ – *p***1** (Gurtin, 1981) and the remaining variables defined as before.

3.2 A (d-*p*-u) multi-field stabilized formulation

Over the fluid domain $\overline{\Omega}$, a finite element partition Ω^h consisting of convex quadrilateral elements in $\Re^2$ was performed in the usual way (Ciarlet, 1978), In order to approximate extra-stress, pressure and velocity fields, respectively, the following finite-element spaces have been employed,

$$\Sigma^h=\{\mathbf{S}\in C^0(\Omega)^{NxN}\cap L_2(\Omega)^{NxN}|S_{ij}=S_{ji},\ i,j=1,N\ |S_K\in R_k(K)^{NxN},\ K\in\Omega^h\}$$
$$P^h=\{q\in C^0(\Omega)\cap L_2^0(\Omega)|q_K\in R_l(K),\ K\in\Omega^h\}$$
$$\mathbf{V}^h=\{\mathbf{v}\in H_0^1(\Omega)^N|\mathbf{v}_K\in R_m(K)^N,\ K\in\Omega^h\} \qquad (7)$$
$$\mathbf{V}_g^h=\{\mathbf{v}\in H^1(\Omega)^N|\mathbf{v}_K\in R_m(K)^N,\ K\in\Omega^h,\ \mathbf{v}=\mathbf{u}_g\text{ on }\Gamma_g\}$$

where R_k, R_l and R_m denote the polynomial spaces of degrees *k, l* and *m* , respectively (Ciarlet, 1978).

Based on the finite element subspaces defined by Eq. (7), a multi-field stabilized formulation for Eq. (6) may be written as: *given the body force **b** and boundary condition **u**_g, find the triple* $(\mathbf{d}^h, p^h, \mathbf{u}^h)\in \Sigma^h$ x P^h x V_g^h *such that:*

$$B(\mathbf{d}^h,p^h,\mathbf{u}^h;\mathbf{S}^h,q^h,\mathbf{v}^h)=F(\mathbf{S}^h,q^h,\mathbf{v}^h) \qquad \forall(\mathbf{S}^h,q^h,\mathbf{v}^h)\in\Sigma^h\times P^h\times V^h \qquad (8)$$

where

$$B(\mathbf{d}^h,p^h,\mathbf{u}^h;\mathbf{S}^h,q^h,\mathbf{v}^h)=\int_\Omega\mathbf{d}^h\cdot\mathbf{S}^h d\Omega-\int_\Omega\mathbf{D}(\mathbf{u}^h)\cdot\mathbf{S}^h d\Omega+\int_\Omega\rho[\nabla\mathbf{u}^h]\mathbf{u}^h\cdot\mathbf{v}^h d\Omega+\int_\Omega 2\eta(R_r,II_{\mathbf{D}})\mathbf{d}^h\cdot\mathbf{D}(\mathbf{v}^h)d\Omega$$
$$-\int_\Omega 2[\mathbf{d}^h]\nabla(\eta(R_r,II_{\mathbf{D}}))\cdot\mathbf{v}^h d\Omega-\int_\Omega p^h\text{div}\,\mathbf{v}^h d\Omega+\int_\Omega\text{div}\,\mathbf{u}^h q^h d\Omega+\delta\int_\Omega\text{div}\,\mathbf{u}^h\text{div}\,\mathbf{v}^h d\Omega$$
$$+\sum_{K\in\Omega^h}\int_{\Omega_K}(\rho[\nabla\mathbf{u}^h]\mathbf{u}^h+\nabla p^h-2\eta(R_r,II_{\mathbf{D}})\text{div}\,\mathbf{d}^h-2[\mathbf{d}^h]\nabla(\eta(R_r,II_{\mathbf{D}})))\cdot$$
$$\cdot\alpha(\text{Re}_K)(\rho[\nabla\mathbf{v}^h]\mathbf{u}^h-\nabla q^h-2\eta(R_r,II_{\mathbf{D}})\text{div}\,\mathbf{S}^h-2[\mathbf{S}^h]\nabla(\eta(R_r,II_{\mathbf{D}})))d\Omega$$
$$+\beta\sum_{K\in\Omega^h}2\eta(\dot{\gamma})\int_\Omega(\mathbf{d}^h-\mathbf{D}(\mathbf{u}^h))\cdot(\mathbf{S}^h-\mathbf{D}(\mathbf{v}^h))d\Omega$$

$$(9)$$

and

$$F(\mathbf{S}^h,q^h,\mathbf{v}^h)=\int_\Omega\rho\mathbf{b}\cdot\mathbf{v}^h d\Omega+\int_{\Gamma_h}\mathbf{t}\cdot\mathbf{v}^h d\Gamma$$
$$+\sum_{K\in\Omega^h}\int_{\Omega_K}\rho\mathbf{b}\cdot\alpha(\text{Re}_K)(\rho[\nabla\mathbf{v}^h]\mathbf{u}^h-\nabla q^h-2\eta(R_r,II_{\mathbf{D}})\text{div}\,\mathbf{S}^h-2[\mathbf{d}]\nabla(\eta(R_r,II_{\mathbf{D}})))d\Omega \qquad (10)$$

with the stability parameters δ *and* α (Re_K) *associated to continuity and motion equations, respectively, given by (Franca and Frey, 1992),*

$$\delta = |\mathbf{u}|_p \, h_K \, \xi \left(\text{Re}_K \right)$$

$$\alpha \left(\text{Re}_K \right) = \frac{h_K}{2 |\mathbf{u}|_p} \xi \left(\text{Re}_K \right) \quad \text{with} \quad \xi \left(\text{Re}_K \right) = \begin{cases} \text{Re}_K, & 0 \le \text{Re}_K < 1 \\ 1, & \text{Re}_K \ge 1 \end{cases} \tag{11}$$

$$\text{Re}_K = \frac{\rho \, m_K |\mathbf{u}|_p \, h_K}{4 \, \eta \left(R_r, \, II_{\mathbf{D}} \right)} \quad \text{with} \quad m_k = \min \{1/3, 2C_k\} \quad \text{and} \quad C_k \sum_{K \in \Omega^h} h_K^2 \|\text{div} \, \mathbf{S}^h\|_{0,K}^2 \ge \|\mathbf{S}^h\|_K^2 \quad \forall \mathbf{S}^h \in \Sigma^h$$

and $|\mathbf{u}|_p$ stands for the p-norm on $\Re^N$, C_k a constant independent of mesh size, h_K, derived from the inverse estimate (Franca and Frey, 1992) and the stability parameter β from the material equation set equal to 0.25, according to Behr et al. (1983).

Remark: The multi-field formulation defined by Eq. (8)-(11) is a Galerkin Least-squares-like formulation based on the the GLS formulation introduced in Behr et al. (1993).

3.3. Non-linear matrix problem

Discretization of Eq. (8) has been carried out by expanding the trial functions (**d**-*p*-**u**), and their respective test functions (**S**-*q*-**v**)*,* in terms of finite element shape functions. This leads to a set of discrete equations, which, in the residual form is written as:

$$\mathbf{R}(\mathbf{U}) = \mathbf{0} \tag{12}$$

where **U** is vector of degrees of freedom for $\mathbf{d}^h$, $\mathbf{u}^h$ and p^h associated to the mesh nodal points. In two-dimensional planar cases, it assumes the form $\mathbf{U} = [\mathbf{d}_{12}, \mathbf{d}_{11}, \mathbf{d}_{22}, u_1, u_2, p]^T$ and the residual $\mathbf{R}(\mathbf{U})$ is given by the following matrix expression,

$$\mathbf{R}(\mathbf{U}) = [\mathbf{E} + \mathbf{E}_\alpha (\mathbf{u}, \eta (R_r, II_{\mathbf{D}})) + \mathbf{H}] \mathbf{d} + [\mathbf{N}(\mathbf{u}) + \mathbf{N}_\alpha (\mathbf{u}, \eta (R_r, II_{\mathbf{D}})) + \mathbf{K}_\alpha (\mathbf{u}, \eta (R_r, II_{\mathbf{D}})) + \mathbf{H}^T - \mathbf{G}^T + \delta] \mathbf{u}$$
$$+ [\mathbf{G} + \mathbf{G}_\alpha (\mathbf{u}, \eta (R_r, II_{\mathbf{D}}))] \mathbf{p} - [\mathbf{F} + \mathbf{F}_\alpha (\mathbf{u}, \eta (R_r, II_{\mathbf{D}}))] \tag{13}$$

where [**H**] is the matrix derived from the surface force term of motion, and [**H**ᵀ] the matrix from the stress-deformation relation term of material equation, [**E**] the matrix from extra-stress term of material equation, [**N**] the matrix from the inertia force term of motion equation, [**K**] the matrix from the diffusive term of material equation, [**G**] and [**G**ᵀ] the matrices from the pressure term of motion equation and incompressibility term of continuity equation, respectively, [**F**] the matrix from the body force term of motion equation. Matrices subjected to α-subscript denote are derived from stabilized terms of motion equation, [**δ**] is the matrix from δ-stabilized-term of continuity.

To solve the residual matrix problem defined by Eq. (12)-(13), a Newton-like incremental method has been employed. This algorithm may be summarized as follows.

$$\mathbf{J}(\mathbf{U}_k) \mathbf{A}_{k+1} = \mathbf{R}(\mathbf{U}_k) \tag{14}$$

with the residual $\mathbf{R}(\mathbf{U})$ defined by Eq. (13) and the Jacobian matrix $\mathbf{J}(\mathbf{U}_k)$ given by

$$\mathbf{J}(\mathbf{U}_k) = \frac{\partial \mathbf{R}(\mathbf{U}_k)}{\partial \mathbf{U}} \tag{15}$$

From Eq. (14), the degree of freedom vector $\mathbf{U}_k$ may be update as

$$\mathbf{U}_{k+1} = \mathbf{U}_k + \mathbf{A}_{k+1} \tag{16}$$

Remark: The convergence criterion adopted in the algorithm defined by Eq. (15)-(17) was the magnitude of the residual $\mathbf{R}(\mathbf{U}_k)$ less than 10^{-7}. As initial solution estimates, null extra-stress, pressure and velocity fields were adopted.

4. NUMERICAL RESULTS

In this section. the multi-field stabilized formulation defined by Eq. (8)-(11) was employed to approximate flow-type sensitive quasi-Newtonian fluids. The considered flow geometry consisted of a four-to-one sudden contraction with a rounded corner of curvature radius equal to $3/4L$ – with L standing for width of the narrow part of the channel, as depicted in Fig. 3. For all computations, a combination of bi-quadratic/bi-linear/bi-quadratic finite element

interpolations (Q2/Q1/Q2) has been used to approximate strain rate, pressure and velocity, respectively. After a mesh independence test, a finite element mesh consisting of 2,670 finite elements – which rendered 11,219 nodal points - has been chosen and employed in all numerical simulations.
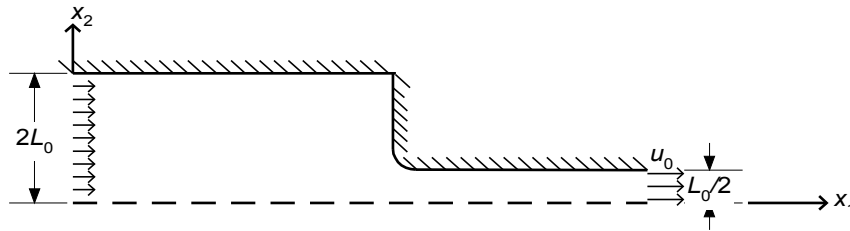
Figure 3. Flow through a four-to-one sudden contraction with rounded corner: problem statement.

The characteristic strain rate, $\dot{\gamma}_c$, was assumed to be the relationship between the outlet average velocity, u_0, and the half width $L/2$. Hence, the Deborah number may be defined by for flow-sensitive fluids may be expressed by (Ryssel and Brunn, 1999):

$$\mathrm{De}_i = \lambda_i \, \dot{\gamma}_c = \frac{2\,\lambda_i u_0}{L} \tag{17}$$

where subscript i is related to extensional ($i=ex$) or shearing ($i=s$) viscosity functions given by Eq. (3). In the numerical simulations, all the investigated fluids had the same value of λ either for pure shearing (λ_s) or pure extension (λ_{ex}). Hence, both shearing and extensional Debora numbers have been fixed as $\mathrm{De}_s = \mathrm{De}_{ex} = 0.6$, respectively, and the Reynolds numbers has been set equal to one in all simulated flows. Three different flow-type sensitive fluids have been considered in the numerical simulations, namely (a) a shear-thinning fluid,with $n_s = 0.1$ and $n_{ex} = 1.0$, (b) a shear-thinning and extension-thickening fluid, with $n_s = 0.5$ and $n_{ex} = 1.5$, and (c) an extension-thickening fluid, with $n_s = 1.0$ e $n_{ex} = 2.5$.
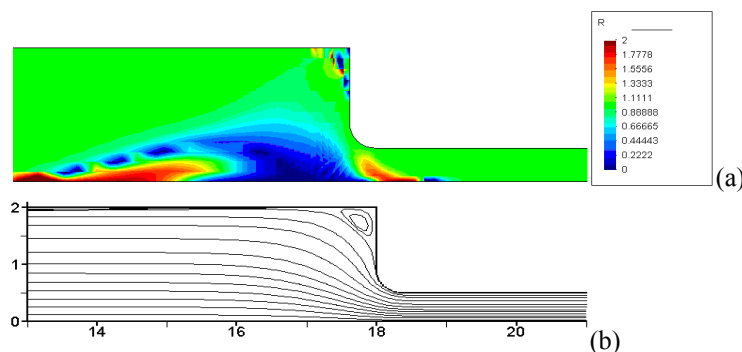
Figure 4. Newtonian fluid flow: (a) flow classifier distribution R_r and (b) flow streamlines in the contraction corner.

The Fig. 4a shows, for a Newtonian fluid, the distribution of the flow classifier R_r along the channel. It may be noticed that the classifier R_r had a unity value for the greater portion of the channel, $i.$ $e.$, the Newtonian flow may be classified as a shear-dominated one. However, in the contraction entrance , an extensional zone ($R_r=0$) may be observed due to channel straitening. Besides, some rigid body ($R_r \to 2$) zones may be still observed near the contraction corner, in which a small vortex – due to the low Reynolds value – has been captured as illustrated by the flow streamlines of Fig. 4b.

In Fig. 5, the dimensionless viscosity fields, $\eta^* = \eta/\eta_0$, for the three investigated fluids, have been presented. For the shear-thinning fluid illustrated in Fig. 5a, it may be verified a viscosity decay ($\eta^* < 1$) near the wall of the smaller channel – a region subjected to high shear rates. At contraction entrance, a region typically subjected to extensional flow, the viscosity did not decay even for high shear rates, due to the values of the flow classifier, R_r, got closer to zero. In Fig. 5b, for the shear-thinning and extension-thickening fluid, a viscosity increasing ($\eta^* > 1$) may be verified at extensional region near the contraction entrance and a viscosity reduction ($\eta^* < 1$) at shear zone near the wall channel. In Fig. 5c, for the extension-thickening fluid, the only viscosity increasing ($\eta^* > 1$) has occurred in the region subjected to an extensional kinematics, i $.e.$, the one near the contraction entrance. In all other regions of Fig. 5c, the viscosity distribution has remained constant.
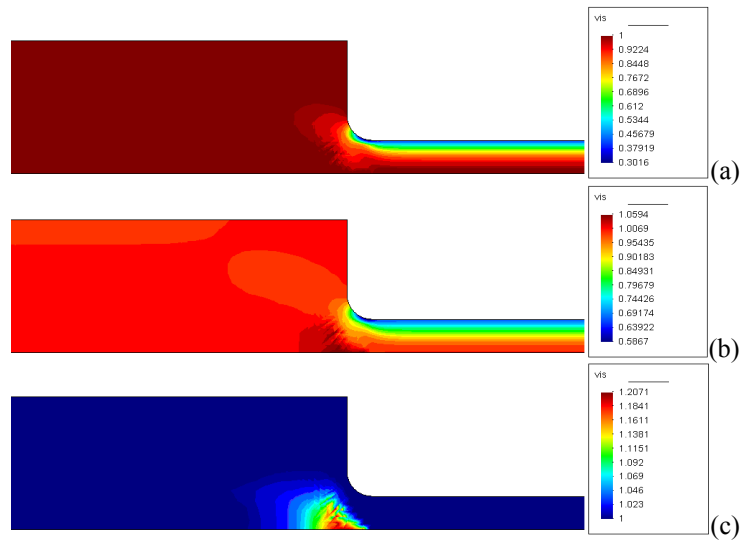
Figure 5. Viscosity function for (a) n_s=0.1 and n_{ex}=1.0; (b) n_s=0.5 and n_{ex}=1.5; (c) n_s=1.0 and n_{ex}=2.5.

Figure 6 shows the dimensionless velocity profiles, $u^*=u_1/u_0$, for four distances from the contraction plane: Fig. 6a presents fully-developed velocity profiles upstream of the contraction, Fig. 6b and 6c velocity profiles just upstream of the contraction − with the latter figure depicting a detail of the profiles near the symmetry line − and Fig. 6d velocity profiles just after the entrance of the smallest channel, and Fig. 6e the fully developed velocity profile in the narrow channel.

(e)
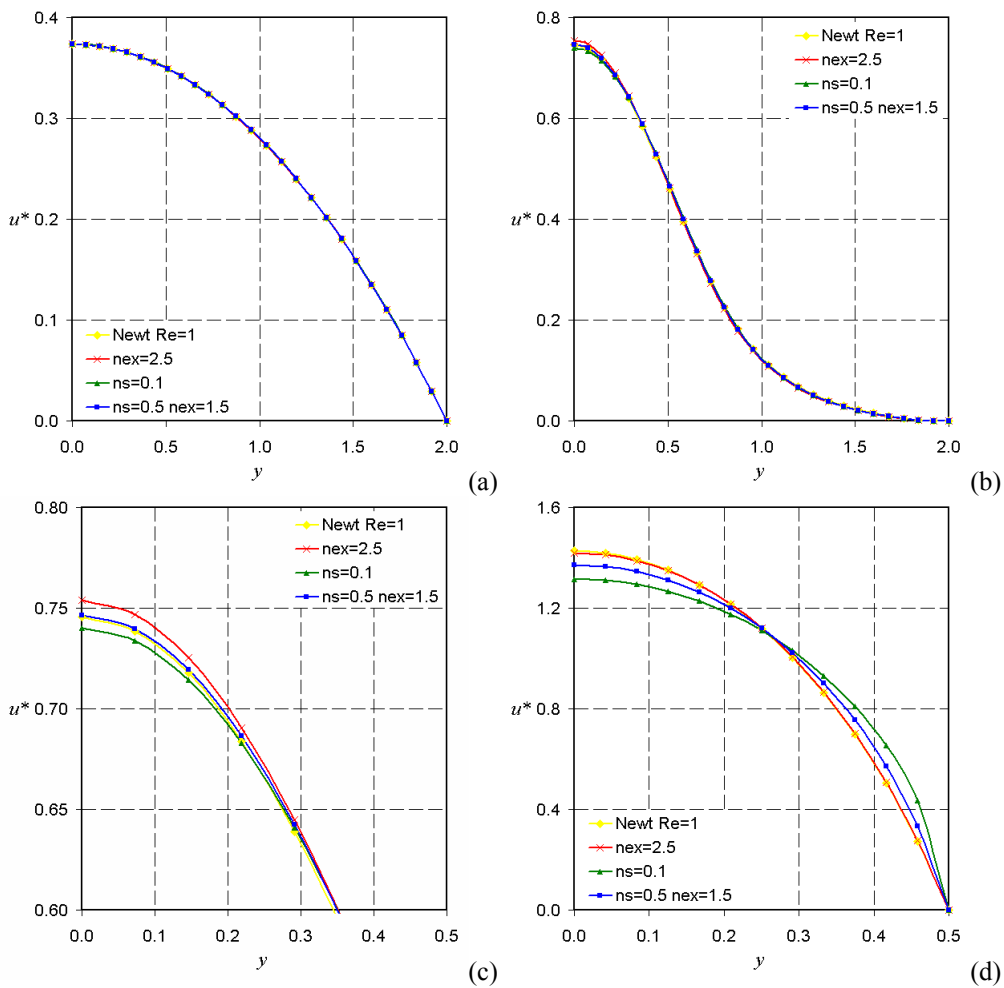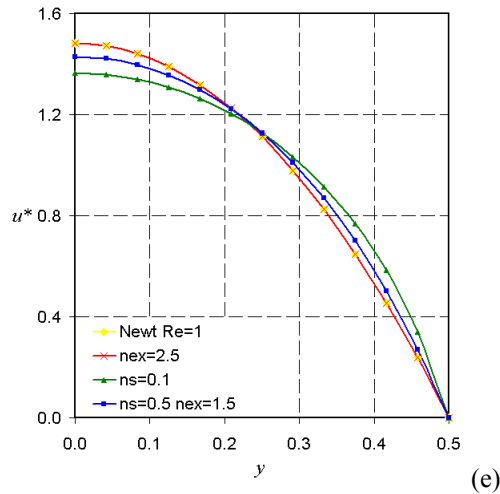
Figure 6. Velocity profiles: (a) $-11L$; (b) $-0.5L$; (c) $-0.5L$ (zoom); (d) $0.375L$, (e) $2.5L$.

In Fig. 6a, all the studied fluids have presented similar velocity profiles, due to all the three flows were not disturbed yet by elliptical effects emanated from by the downstream contraction. Even this region being a shear-dominated one, the strain rates were not sufficient high that shear-shinning effects could significantly affect the fluid dynamics of low Deborah flows (De=0.6). In Fig. 6b, it may be noticed very similar velocity profiles, too. However, the detail near the symmetry line showed in Fig. 6c gave risen to some distinctness: (a) the shear-thinning fluid (n_s=0.1 and n_{ex}=1.0) showed a flatter profile, (b) the shear-thinning and extension-thickening fluid (n_s=0.5 and n_{ex}=1.5), a more elongated one, with the maximum velocity a little high than the Newtonian fluid, (c) the extensional-thickening fluid (n_s=1.0 e n_{ex}=2.5), the highest maximum velocity at symmetry line. In the contraction region, the flow classifier R_r approached to null values at symmetry line characterizing, in this way, an extensional region. Hence, the viscosity increasing near the symmetry line was responsible by the increasing of the maximum velocity, while viscosity reduction became the velocity profiles flatters. Finally, In Fig. 6d may be found almost flat velocity profiles for the shear-thinning fluid. As it may be observed, just downstream the contraction, that the high shear rates experimented in smaller channel were already able to generate a shear-dominated region, phenomenon which is corroborated in Fig. 6e, farther from the contraction.

Fig. 7 shows dimensionless normal extra-stress profiles, $\tau_{11}{}^*=(\tau_{11}L)/(\eta_0 u_0)$ and $\tau_{22}=(\tau_{22}L)/(\eta_0 u_0)$, along the symmetry line. For the extensional-thickening fluid (n_{ex}=2.5), it may be verified an increasing of normal extra-stresses due to the need to surpass the additional flow resistance imposed by the increasing of the extensional viscosity at the contraction entrance – a region subject to an extensional kinematics. For the shear-thinning fluid (n_s=0.1), the normal extra-stresses were lower than those of the Newtonian fluid, in virtue of a lower extra-stress distribution induced by the shearing viscosity reduction near the contraction – a decay that has even influenced the extra-stress distribution on the extensional region at symmetry line. At length, for the shear-thinning and extension-thickening fluid (n_s=0.5 and n_{ex}=1.5), the low viscosities at shearing regions and high viscosities at extensional ones have prescribed an intermediate behavior between the pure extensional-thickening and pure shear-thinning fluids. Indeed, its extra-stresses were only a little lower than the Newtonian ones.

(a)

(b)
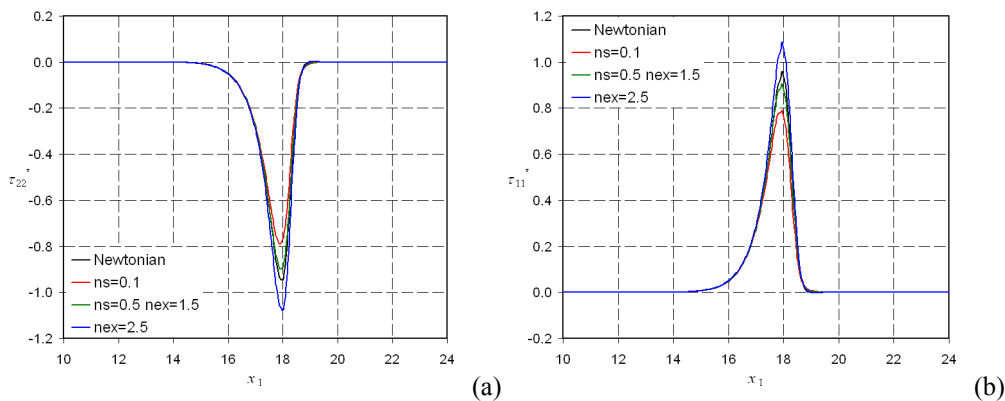
Figure 7. (a) $\tau_{11}{}^*$ and (b) $\tau_{22}{}^*$ profiles through on the symmetry line of the flow.

5. FINAL CONCLUSIONS

In this article, flow-type sensitive quasi-Newtonian fluid flows have been numerically investigated. The mechanical model employed the mass conservation and momentum balance equations coupled with a quasi-Newtonian viscosity function, dependent of the second invariant of the strain rate tensor and a kinematic flow classifier. According to the value of the flow classifier, the mechanical model could accommodate either shear-thinning or extension-thickening in mixed or pure type flow regions. Some two-dimensional simulations of low Deborah flows have been carried out through a four-to-one sudden contraction with a rounded corner. Four distinct fluids have been investigated: a Newtonian, a shear-thinning, an extensional thickening and a shear-thinning and extensional thickening fluid. For all fluid flows, the flow classifier distribution has indicated an extensional region in the contraction vicinity and pure shear flow far away the contraction. Besides, at contraction entrance, it was observed that the most extensional flows have generated more elongated velocity profiles, while the most shear-thinning fluids generated flatter ones. In addition, at region just downstream of the contraction, the shear-thinning were even flatter. On the other hand, far away and upstream of the contraction, all velocity profiles have been very similar, due to the low shear rates experimented on those regions. At last, for regions far away the contraction, null normal extra-stresses along the symmetry line have been obtained, indicating fully-development flow regions. For the contraction vicinity, the normal extra-stress have jumped near the symmetry line, with positive values for τ_{11} and negative ones for τ_{22}. For these regions, the more extensional-thickening the fluid, the higher the normal stress peaks, in virtue of these fluids experiment a viscosity increasing at extensional regions.

6. ACKNOWLEDGEMENTS

7. REFERENCES

Astarita, G., 1979, "Objective and generally applicable criteria for flow classification", J. Non-Newtonian Fluid Mech., Vol. 6, pp. 69–76.

Astarita, G., 1991, "Quasi-Newtonian constitutive equations exhibiting flow-type sensitivity", J. Rheology, Vol. 35, pp. 687-689.

Behr, M., Franca, L.P., Tezduyar, T.E., 1993, "Stabilized finite element methods for the velocity-pressure-stress formulation of incompressible flows", Comput. Methods Appl. Mech. Engrg., Vol. 104, pp. 31-48.

Ciarlet, P. G., 1978, "The finite element method for elliptic problems". North Holland, Amsterdam.

Franca, L.P. and Frey, S., 1992, "Stabilized finite element methods: II. The incompressible Navier-Stokes equations". Computer Methods in Applied Mechanics and Engineering,. Vol. 99, pp. 209-233.

Gurtin, M. E., 1981, "An Introduction to Continuum Mechanics". Academic Press, New York, U.S.A.

Ryssel, E., Brunn, P.O., 1999, "Flow of a quasi-Newtonian fluid through a planar contraction", J. Non-Newtonian Fluid Mech., Vol. 85, pp. 11-27.

Schunk, P. R., Scriven, L. E., 1990. "Constitutive equation for modeling mixed extension and shear in polymer solution processing", J. Rheology, Vol. 34 (7), pp. 1085-1119.

Souza Mendes, P.R., Padmanabhan, M., Scriven, L. E., Macosko, C.W., 1995, "Inelastic constitutive equations for complex flows", Rheologica Acta, Vol. 34, pp. 209-214.

Thompson, R.L. and Souza Mendes, P. R., 2005, "Persistence of straining and flow classification", International Journal of Engineering Science, pp. 79-105.

Thompson, R.L., Souza Mendes, P.R., Naccache, M.F., 1999. "A new constitutive equation and its performance in contraction flows", J. Non-Newtonian Fluid Mech., Vol.86, pp. 375-388.

8. RESPONSIBILITY NOTICE